

Reliable Optimization Under Noise in Quantum Variational Algorithms

Vojtěch Novák^{1,2}, Silvie Illésová⁶, Tomáš Bezděk³, Ivan Zelinka^{2,4}, and Martin Beseda⁵

¹ Department of Computer Science, Faculty of Electrical Engineering and Computer Science,

VSB - Technical University of Ostrava, Ostrava, Czech Republic
 vojtech.novak.st1@vsb.cz

² IT4Innovations National Supercomputing Center,

VSB - Technical University of Ostrava, 708 00 Ostrava, Czech Republic

³ Department of Mathematics, TUM School of Computation, Information and Technology, Technical University of Munich, Garching bei München, Germany

⁴ Department of Informatics and Statistics, Marine Research Institute, Klaipeda University, Lithuania

⁵ Dipartimento di Ingegneria e Scienze dell'Informazione e Matematica, Università dell'Aquila, Via Vetoio, I-67010 Coppito, L'Aquila, Italy

⁶ Gran Sasso Science Institute, L'Aquila, Italy

Abstract. The optimization of Variational Quantum Eigensolver is severely challenged by finite-shot sampling noise, which distorts the cost landscape, creates false variational minima, and induces statistical bias called winner's curse. We investigate this phenomenon by benchmarking eight classical optimizers spanning gradient-based, gradient-free, and metaheuristic methods on quantum chemistry Hamiltonians H_2 , H_4 chain, LiH (in both full and active spaces) using the truncated Variational Hamiltonian Ansatz. We analyze difficulties of gradient-based methods (e.g., SLSQP, BFGS) in noisy regimes, where they diverge or stagnate. We show that the bias of estimator can be corrected by tracking the *population mean*, rather than the biased best individual when using population based optimizer. Our findings, which are shown to generalize to hardware-efficient circuits and condensed matter models, identify adaptive metaheuristics (specifically CMA-ES and iL-SHADE) as the most effective and resilient strategies. We conclude by presenting a set of practical guidelines for reliable VQE optimization under noise, centering on the co-design of physically motivated ansatz and the use of adaptive optimizers.

Keywords: Quantum computing, Variational Quantum Eigensolver, Differential Evolution, Noisy Optimization, Evolutionary optimization

1 Introduction

Optimization under stochastic noise presents a universal challenge in numerical and physical sciences. In black-box optimization, where the objective function

is accessed only through noisy evaluations, random fluctuations can distort the apparent topology of the loss landscape. Additive Gaussian noise leads to a statistical phenomenon known as the *winner's curse*, where the lowest observed energy or cost is biased downward relative to the true expectation value due to random fluctuations [1, 36]. This bias results in the optimizer prematurely accepting a spurious minimum as the global optimum, preventing the discovery of better, higher accuracy solutions. When applied to quantum variational algorithms, this stochastic effect acquires deeper physical implications. In the context of the Variational Quantum Eigensolver (VQE) [7], the cost function is the variational expectation value

$$C(\boldsymbol{\theta}) = \langle \psi(\boldsymbol{\theta}) | \hat{H} | \psi(\boldsymbol{\theta}) \rangle, \quad (1)$$

where $|\psi(\boldsymbol{\theta})\rangle = U(\boldsymbol{\theta})|0\rangle$ is the variational ansatz prepared by the parameterized unitary $U(\boldsymbol{\theta})$ acting on an easy to prepare reference state $|0\rangle$. The cost function should be bounded by the variational principle from below by the true energy of the ground state, $C(\boldsymbol{\theta}) \geq E_0$. However, in practice, we can only estimate the expectation value of the cost function up to a finite precision determined by the number of measurement shots, N_{shots} . The corresponding estimator reads

$$\bar{C}(\boldsymbol{\theta}) = C(\boldsymbol{\theta}) + \epsilon_{\text{sampling}}, \quad (2)$$

where $\epsilon_{\text{sampling}}$ is a zero-mean random variable, typically modeled as Gaussian noise, $\epsilon_{\text{sampling}} \sim \mathcal{N}(0, \sigma^2/N_{\text{shots}})$. This sampling noise can lead to apparent violations of the variational bound, yielding $\bar{C}(\boldsymbol{\theta}) < E_0$, a phenomenon known as *stochastic variational bound violation*.

This appears as false variational minima, illusory states that seem better than the true ground state, but arise solely from statistical fluctuations [46, 28]. These minima can mislead the optimizer, inducing premature convergence or divergence depending on the search strategy. This effect is further compounded by the presence of a *noise floor*, a finite lower limit in achievable precision defined by the sampling variance of the observable [28].

Another fundamental trainability limitation of VQE arises from the *Barren Plateau (BP)* phenomenon [24]. In the presence of BPs, gradients of the loss function or equivalently expectation differences concentrate exponentially around their mean with increasing the number of qubits, rendering the landscape effectively flat and featureless. The loss function can be expressed in operator form as

$$\ell_{\boldsymbol{\theta}}(\rho, O) = \text{Tr}[\rho(\boldsymbol{\theta})O], \quad (3)$$

where $\rho(\boldsymbol{\theta}) = U_{\boldsymbol{\theta}}(\rho)$ and $\rho = |\psi\rangle\langle\psi|$ is the density matrix. Equation (3) can be interpreted using the Hilbert-Schmidt inner product $\langle A, B \rangle = \text{Tr}[A^\dagger B]$, so that $\ell_{\boldsymbol{\theta}}(\rho, O) = \langle \rho(\boldsymbol{\theta}), O \rangle$ represents the overlap between two operators viewed as vectors in the operator space $B(\mathcal{H}_0)$ of dimension 4^n . Optimization can thus be viewed as the anti-alignment of these two exponentially large vectors, which far exceeds the Hilbert space dimension 2^n . As discussed in the BP review [24],

this exponential operator space structure fundamentally limits trainability, producing exponentially vanishing gradients and effectively concealing the direction of improvement under any finite sampling precision.

Recent work has broadened the VQE framework to include advanced variants such as the State-Averaged Orbital-Optimized VQE (SAOOVQE), allowing ground and excited-state descriptions under realistic quantum noise conditions [3, 19, 21, 35]. The reliability of variational optimization under noise is likewise relevant beyond quantum chemistry, influencing quantum machine learning [17, 18, 12], condensed-matter modeling [44, 9], and emerging practical uses such as medical diagnostics [30, 31] and software testing [40, 15].

In this work, we extend our previous investigation of optimization strategies for the truncated Variational Hamiltonian Ansatz (tVHA) [20] by broadening the scope to multiple ansatz types and physical models. Our aim is to provide the reader with a clearer intuition for how finite-shot sampling noise reshapes variational energy landscapes across both problem-inspired (tVHA) and hardware-efficient (TwoLocal) circuits. Using molecular (H_2 , H_4 , LiH with full and active space), Ising, and Fermi–Hubbard systems, we visualize how smooth convex basins deform into rugged multimodal surfaces as noise increases. These visualizations, together with systematic benchmarks, expose how different optimizers respond to stochastic distortions in the loss landscape.

We benchmarked gradient-based, gradient-free, and evolutionary optimizers under identical noise conditions. Gradient-based methods (gradient descent, Sequential Least Squares Programming (SLSQP) [5, 23], Broyden-Fletcher-Goldfarb-Shanno Algorithm (BFGS) [26]) rapidly lose stability once the cost curvature approaches the sampling noise level, producing unreliable gradient and Hessian estimates. Population-based methods (Covariance Matrix Adaptation Evolution Strategy (CMAES), PSO [10, 27]) remain functional through implicit averaging but suffer from the *winner’s curse*, showing false improvements unless high-shot reevaluation is used [1, 36]. This motivates statistically grounded acceptance rules and adaptive resampling in noisy variational optimization.

Importantly, these effects are not specific to the tVHA or to quantum chemistry. Our complementary study on the 1D Ising and Fermi–Hubbard models using a hardware-efficient TwoLocal ansatz [32] reveals the same phenomena: gradient-based optimizers have difficulties converging, and finite-shot noise converts smooth basins into rugged, multimodal landscapes. Observing identical behaviors across two distinct ansatz classes (physically motivated tVHA versus generic TwoLocal) and across domains (molecular chemistry versus condensed matter) suggests that these stochastic distortions and optimizer failures are *generic features* of noisy VQE, situating our results within a broader framework of noisy hybrid optimization [28, 46].

The tVHA ansatz itself mitigates barren plateaus through compact, physically motivated structure and initialization near the Hartree–Fock state, ensuring polynomially decaying gradients [20, 33]. This distinguishes it from hardware-efficient circuits and makes ansatz design a concrete *noise-mitigation strategy*.

In summary, Section 1 introduces the motivation and theoretical background, emphasizing stochastic variational bound violations and barren plateaus in VQE. Section 2 outlines the analytical and numerical methods, including stochastic bias modeling, benchmark Hamiltonians, and the construction of the tVHA and TwoLocal circuits, we also relate optimizer step sizes to the Hessian spectrum, showing that when steps exceed local curvature scales, noise dominates updates. Section 3 presents results that compare classical optimizers with varying noise levels, while Section 4 summarizes results from all systems studied, the role of structured ansatz design, and the advantages of adaptive evolutionary methods. Appendix A lists the implementation details and reproducibility settings.

2 Methods

This section outlines the analytical and numerical techniques used to characterize the impact of finite sampling on variational quantum optimization. We first quantify how measurement noise introduces *stochastic selection bias* and generates false minima, establishing a statistical framework for evaluating bias magnitude and noise floors. We then analyze how this stochasticity reshapes the underlying VQE optimization landscape, examining its interplay with circuit expressivity, ansatz structure, and optimizer behavior under realistic shot noise.

2.1 Stochastic selection bias and false minima under finite sampling

Variational quantum algorithms (VQAs) rely on parameterized quantum circuits (PQCs), also called ansatz, to generate states of the form

$$|\psi(\boldsymbol{\theta})\rangle = U(\boldsymbol{\theta})|0\rangle, \quad (4)$$

where the unitary transformation can be expressed as a sequence of parameterized layers

$$U(\boldsymbol{\theta}) = \prod_{i=1}^L U_i(\theta_i), \quad (5)$$

with $\boldsymbol{\theta} = (\theta_1, \dots, \theta_L)$ representing trainable parameters. These parameters can be interpreted as effective evolution times under the corresponding generators, for example $U(\theta) = e^{-i\theta H}$.

The objective of the algorithm is to minimize the cost function defined in Eq. (1). However, as shown in Eq. (2), in practice the expectation value can only be estimated up to finite precision determined by the number of measurement shots, N_{shots} . For a molecular Hamiltonian decomposed into Pauli strings $\hat{H} = \sum_k c_k P_k$, the intrinsic variance follows

$$\text{Var}[C(\boldsymbol{\theta})] = \langle \hat{H}^2 \rangle - \langle \hat{H} \rangle^2, \quad (6)$$

with covariance contributions arising within commuting groups used to reduce the measurement count.

Each function evaluation (FE) in the optimization corresponds to one noisy estimate $\bar{C}(\boldsymbol{\theta}_i)$ computed from N_{shots} samples. The optimization algorithm then selects the smallest of K such draws:

$$\bar{C}_{\min} = \min_{i \in \{1, \dots, K\}} \bar{C}(\boldsymbol{\theta}_i). \quad (7)$$

Even though $\mathbb{E}[\epsilon_{\text{sampling}}] = 0$, the statistical minimum \bar{C}_{\min} is biased downward because the minimum of noisy random variables systematically overestimates improvement. Following extreme-value statistics [1], the expected bias magnitude scales as

$$\mathbb{E}[\bar{C}_{\min}] - C_{\min} \approx -\sigma_{\text{noise}} \sqrt{2 \log K} \quad (8)$$

where K is the number of function evaluations. In practice, correlated measurements reduce the number of statistically independent samples, effectively lowering K and hence the true bias [2]. For large evaluation counts, one or more noisy estimates will almost certainly fall several standard deviations below the mean, creating false minima; improvements smaller than about four to five noise standard deviations should therefore be treated as statistically insignificant.

The noise floor for each configuration was computed as

$$\sigma_{\text{noise}} = \sqrt{\frac{\bar{\sigma}^2}{N_{\text{shots}}}}, \quad (9)$$

where $\bar{\sigma}^2$ denotes the mean variance of all Hamiltonian evaluations during optimization. For shot counts below a few thousand, the noise floor already exceeds the typical energy improvement step, implying that observed minima below the ground-state reference are spurious statistical outliers rather than physical convergence.

2.2 Model Hamiltonians and Ansatzes

We benchmarked our optimization strategies using two classes of Hamiltonians and corresponding variational ansatzes. The 1D Ising and 6-site Fermi–Hubbard models were simulated using the *TwoLocal* ansatz, while molecular systems (H_2 , H_4 chain and LiH) used tVHA.

The 1D Ising Hamiltonian without external field is defined as

$$H = - \sum_{i=1}^{n-1} \sigma_z^{(i)} \sigma_z^{(i+1)}, \quad (10)$$

where $\sigma_z^{(i)}$ denotes the Pauli- Z operator acting on qubit i , and n is the total number of qubits representing the spin chain [25].

The 6-site Fermi–Hubbard model combines kinetic and on-site interaction terms,

$$H = -t \sum_{\langle i,j \rangle, s} (c_{i,s}^\dagger c_{j,s} + c_{j,s}^\dagger c_{i,s}) + U \sum_i n_{i,\uparrow} n_{i,\downarrow}, \quad (11)$$

where $c_{i,s}^\dagger$ ($c_{i,s}$) are fermionic creation (annihilation) operators for spin $s \in \{\uparrow, \downarrow\}$ at site i , $\langle i, j \rangle$ denotes nearest-neighbor pairs of lattice sites, $n_{i,s} = c_{i,s}^\dagger c_{i,s}$ is the number operator, and $t = U = 1$ [16]. Both the Ising and Hubbard models were used to evaluate optimizer performance on structured yet nontrivial quantum landscapes.

For molecular systems, we used the tVHA, which mitigates the limitations of traditional quantum chemistry ansatzes such as UCC that often lead to deep, non-commuting circuits and exponential parameter scaling. The tVHA is systematically derived from the molecular Hamiltonian

$$H = \sum_{ij} h_{ij} a_i^\dagger a_j + \frac{1}{2} \sum_{ijkl} g_{ijkl} a_i^\dagger a_j^\dagger a_k a_\ell, \quad (12)$$

where a_i^\dagger (a_i) are fermionic creation (annihilation) operators acting on orbital i , h_{ij} are one-electron integrals representing kinetic and nuclear-attraction contributions, and g_{ijkl} are two-electron integrals describing electron–electron interactions. A truncation parameter p limits weaker non-Coulomb terms by retaining only the dominant subset that preserves a chosen fraction of the total interaction strength. The Variational Hamiltonian Ansatz (VHA) and its truncated variants have been extensively analyzed in the context of entanglement, optimization, and expressivity [47, 33, 34, 20].

2.3 VQE optimization landscape: geometry, noise, and step-size stability

The geometry of the variational landscape governs VQE trainability and optimizer robustness. In the noiseless regime, structured ansatzes such as the tVHA form smooth, locally convex basins around the Hartree–Fock initialization, while hardware-efficient circuits (e.g., TwoLocal) introduce mild curvature irregularities. Strongly correlated models like the six-site Hubbard system are inherently multimodal even under exact simulation [6, 45]. Figure 1 compares these topologies, showing two-dimensional parameter slices where only selected parameters vary and others are fixed at their optimized values.

The connection between local curvature and optimizer stability can be made explicit by analyzing the Hessian. Near an optimum $\boldsymbol{\theta}_*$, the cost function can be expanded as

$$C(\boldsymbol{\theta}) \approx C(\boldsymbol{\theta}_*) + \frac{1}{2}(\boldsymbol{\theta} - \boldsymbol{\theta}_*)^\top \mathbf{H}(\boldsymbol{\theta} - \boldsymbol{\theta}_*), \quad (13)$$

where $\mathbf{H} = \nabla^2 C(\boldsymbol{\theta}_*)$ denotes the local Hessian. Unless stated otherwise, all vector norms and inner products are taken with respect to the standard Euclidean (ℓ_2) geometry.

For gradient descent with step size η , the linearized iteration

$$\boldsymbol{\theta}_{k+1} = \boldsymbol{\theta}_k - \eta \nabla C(\boldsymbol{\theta}_k) \quad (14)$$

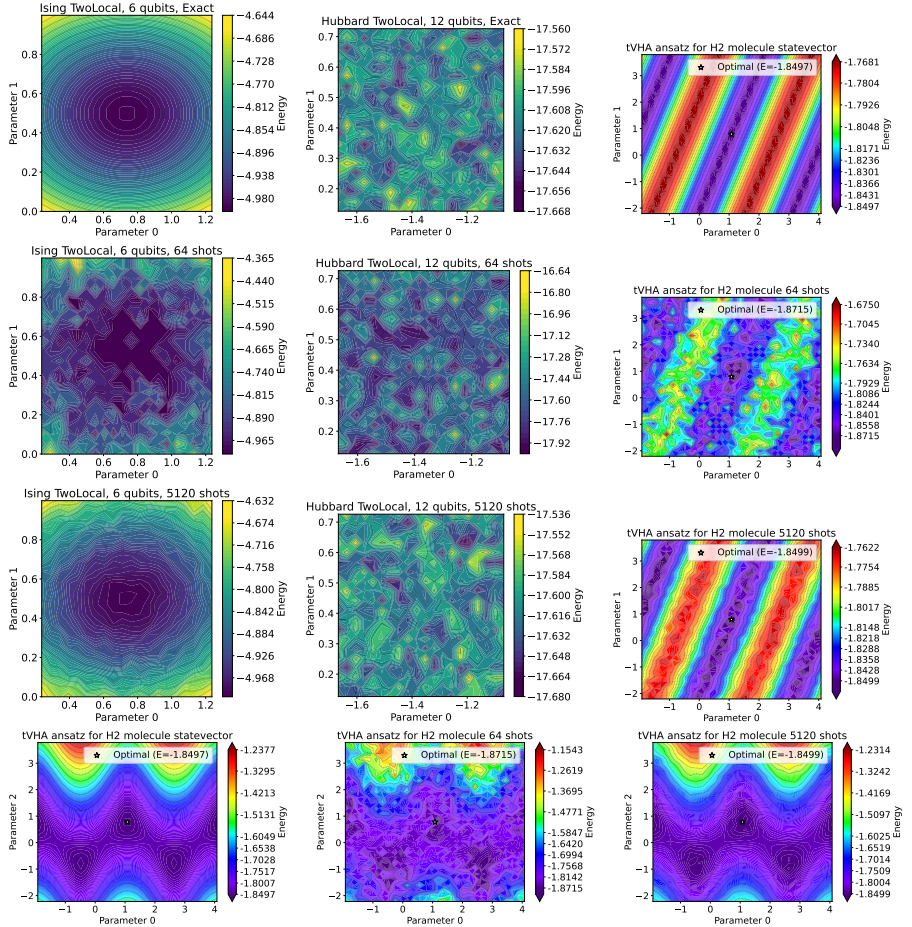


Fig. 1: Combined comparison of energy landscapes across models and noise levels. Columns correspond to the Ising model (left), Hubbard model (center), and H₂ system (right). Rows correspond to statevector/noiseless (top), 64–512-shots (second), 5120–6×1024-shots (third), and alternative H₂ parameter slices (bottom).

is locally stable when the spectral radius of $(\mathbf{I} - \eta \mathbf{H})$ is less than one. For a symmetric positive definite Hessian, this implies

$$0 < \eta < \frac{2}{L}, \quad (15)$$

where $L = \lambda_{\max}(\mathbf{H})$ is the Lipschitz constant of the gradient. The asymptotic convergence rate depends on the condition number $\kappa = L/\mu$, with $\mu = \lambda_{\min}(\mathbf{H})$. A large κ indicates strong anisotropy of the curvature and results in slow convergence along shallow directions.

When finite-shot sampling noise is present, the measured cost $\bar{C}(\boldsymbol{\theta})$ becomes stochastic, and the corresponding gradient estimator satisfies

$$\nabla \bar{C}(\boldsymbol{\theta}) = \nabla C(\boldsymbol{\theta}) + \boldsymbol{\xi}, \quad \mathbb{E}[\boldsymbol{\xi}] = 0, \quad \text{Cov}[\boldsymbol{\xi}] = \Sigma, \quad (16)$$

where $\boldsymbol{\xi}$ represents the random gradient noise arising from finite-shot sampling, modeled as a zero-mean random vector with covariance matrix Σ that quantifies the sampling-induced uncertainty in each gradient component. Once the root-mean-square gradient noise exceeds the local signal scale,

$$\sqrt{\mathbb{E}[\|\boldsymbol{\xi}\|_2^2]} \gtrsim \|\mathbf{H}(\boldsymbol{\theta} - \boldsymbol{\theta}_*)\|_2, \quad (17)$$

the optimizer can no longer reliably detect the descent direction. In this regime dominated by noise, the apparent curvature fluctuates between iterations, so that a fixed step size $\eta \approx 2/L$ alternates between being too small and too large, leading to oscillatory or divergent behavior. Stable operation therefore requires both a well-conditioned Hessian and gradient estimates whose variance is small compared to the curvature scale.

As illustrated in Figure 2, the energy landscape slice for the noisy VQE estimation of the H_2 molecule, using 512 shots with the tVHA ansatz, highlights this issue. The red plane indicates the exact ground-state energy E_0 , but the apparent dips below E_0 arise from the sampling noise, violating the variational principle. These false minima, which emerge due to stochastic fluctuations in the optimization process, emphasize the difficulty of avoiding variational violations in noisy quantum environments. The winner's curse bias exacerbates this issue, causing the optimizer to chase these fluctuations and engage in a random walk that reduces the effectiveness of the optimization process.

Deterministic curvature-based optimizers such as BFGS and SLSQP rely on consistent curvature updates and monotonic objective decrease, so stochastic fluctuations often cause erratic or divergent steps [32, 6]. In contrast, stochastic and population-based strategies, such as SPSA [38] and CMAES [13] average over noisy evaluations, maintaining stability in rugged or noise-dominated landscapes, though they still benefit from periodic high-precision reevaluation of elite candidates.

3 Results

Here we show results for CMAES optimizer in H_2 system using tVHA under various noise settings in Fig. 3. In this part, we analyze the magnitudes of the

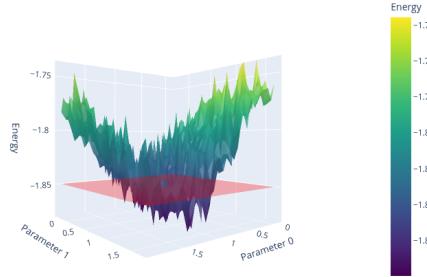


Fig. 2: Energy landscape slice for noisy VQE estimation of H_2 using 512 shots with tVHA ansatz. The red plane indicates the exact ground-state energy E_0 ; apparent dips below E_0 arise from sampling noise, violating the variational principle (false minima).

noise floor σ_{noise} and corresponding errors from tracking the lowest FE in iteration (Best of iterations) compared to averaging all FEs in the iteration (Mean of iterations). Next, we show results for the Ising model in Tab. 1. This table shows how many FEs optimizers needed converge to optimum point in tolerance $1e - 1$ (we show only successful optimizers). After that we present convergence curves of optimizers for the six-site Hubbard model in Fig. 4. Finally, we show convergence curves of optimizers using tVHA in H_2 , H_4 chain, LiH full space and LiH active space systems using random initializations in statevector (exact) and sampling noise simulations.

The results in Fig. 3 demonstrate that combining population-based optimization with averaging across individuals in each iteration significantly suppresses stochastic fluctuations in the energy estimates. The *best of iterations* metric often falls spuriously below the true ground-state energy due to overfitting to random sampling noise, while the population-mean trajectory remains bounded by the empirical noise floor σ_{noise} and follows the expected $1/\sqrt{N_{\text{shots}}}$ scaling. For the CMAES optimizer, this effect is clearly observed across increasing shot numbers. At $N_{\text{shots}} = 64$, the mean absolute error is approximately 4×10^{-3} Ha, compared to 5×10^{-2} Ha for the best-sample metric and a corresponding noise floor of 1.9×10^{-2} Ha. Increasing to $N_{\text{shots}} = 1024$ reduces these values to 1×10^{-3} Ha (mean), 1.6×10^{-2} Ha (best), and 4.2×10^{-3} Ha (σ_{noise}). At $N_{\text{shots}} = 6144$, the mean and noise floor drop to 4×10^{-4} Ha and 1.7×10^{-3} Ha, respectively, and at $N_{\text{shots}} = 30000$ they converge further to 2.5×10^{-4} Ha and 7.4×10^{-4} Ha. This progression confirms that ensemble averaging yields nearly an order of magnitude smaller effective errors than tracking only the best individuals, turning sampling noise from a limiting factor into a statistically manageable uncertainty.

The results in Table 1 demonstrate a clear scaling hierarchy in optimizer efficiency with increasing qubit number. CMAES consistently achieves the fastest convergence across all system sizes, requiring fewer than 3.5×10^3 function evaluations even for nine qubits. The adaptive Improved Success-History Based Parameter Adaptation for Differential Evolution with Linear Population Size

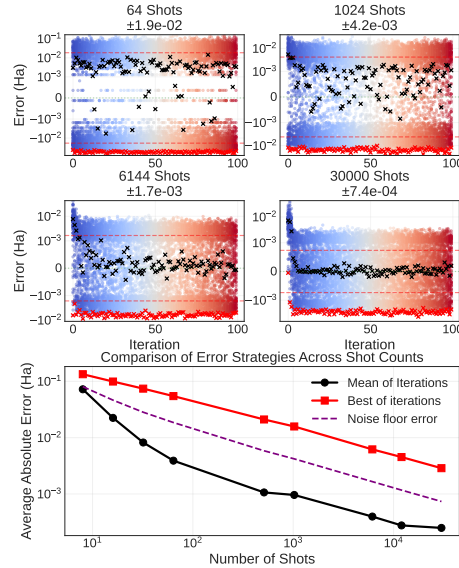


Fig. 3: Energy error from all individuals for H_2 using tVHA. Top: Optimization trajectories (colored points), iteration means (black crosses), best values (red crosses), and noise floors (red dashed lines). Bottom: Average absolute errors for mean-based (black), best-value (red), σ_{noise} (purple).

Reduction (iL-SHADE) follows closely, showing mild growth with system size and maintaining stable convergence within 6.6×10^3 evaluations. Both methods exhibit near linear scaling and robust performance, confirming their ability to adapt search distributions effectively in high-dimensional parameter spaces.

In contrast, Simulated Annealing Cauchy (SA Cauchy) and Harmony Search (HS) show moderate scalability, with function evaluations increasing rapidly beyond seven qubits. Their slower adaptation and limited population diversity lead to premature saturation as the landscape becomes more rugged. DEbest1bin, improved SOMA (iSOMA), and Symbiotic Organisms Search (SOS) [8] perform significantly worse, exhibiting near exponential growth in required evaluations and frequent stagnation at higher dimensions. These results highlight the superior efficiency and scalability of adaptive metaheuristics, particularly CMAES and iL-SHADE, for variational quantum optimization in expanding Hilbert spaces.

The convergence behavior for the six-site Fermi–Hubbard model, shown in Fig. 4, reveals a pronounced separation between adaptive metaheuristics and conventional optimizers under 64-shot sampling noise. Among all tested methods, iL-SHADE and CMAES-ft achieve energies closest to the exact ground state $E_0 = -18$ Ha, reaching final values of -17.984 and -17.998 Ha, corresponding to absolute errors of 1.6×10^{-2} and 2.7×10^{-3} Ha, respectively. Both algorithms maintain smooth, monotonic convergence over the full trajectory, indicating stable adaptation of search distributions even in the presence of measurement noise.

Table 1: Algorithm performance comparison for Ising model without external magnetic field of five to nine qubits. Values represent the mean number of function evaluations (FEs) required for convergence across five independent runs.

Algorithm	5Q	6Q	7Q	8Q	9Q
CMAES	1500	1800	2280	2700	3200
SA Cauchy	3500	4201	7000	8001	9451
iL-SHADE	3274	3333	4368	4374	6559
HS	1740	1726	5046	7066	10586
DEbest1bin	4460	8112	11676	14720	17136
iSOMA	5552	15263	22115	28144	33899
SOS	4880	13440	15320	32000	37843

The unmodified CMAES and SA Cauchy runs converge to slightly higher energies (-17.745 and -17.818 Ha), corresponding to residual errors of 2.6×10^{-1} and 1.8×10^{-1} Ha. Although these methods exhibit consistent early progress, their trajectories plateau prematurely as noise-induced fluctuations obscure curvature information. In contrast, HS and SOS display slower and less stable descent, saturating near -17.08 and -15.73 Ha (errors of 9.2×10^{-1} and 2.27 Ha), suggesting partial trapping in false minima amplified by sampling variance.

Local search and basic evolutionary schemes perform substantially worse. Constrained Optimization By Linear Approximations (COBYLA) terminates near -11.16 Ha, while both DEbest1bin and DEbest1exp stagnate around -10.83 Ha, corresponding to errors exceeding 7 Ha. The iSOMA variant, despite a larger evaluation budget, remains confined above -14.23 Ha, more than 3.7 Ha above the ground state. Such outcomes reflect the inability of fixed-parameter heuristics to cope with the rugged, noise-deformed landscape characteristic of the Hubbard model.

Overall, Fig. 4 demonstrates that only adaptive metaheuristics achieve consistent and near-variational convergence in the noisy Hubbard regime, while deterministic and static search strategies terminate well above the true ground-state energy.

For H_2 , the simplest system, all optimizers except gradient descent converge to near machine precision in noiseless simulations, with BFGS, CMAES, COBYLA, Nelder–Mead, and PSO reaching errors below 10^{-13} – 10^{-14} Ha. Gradient descent and SPSA are slower, with final errors of $\sim 10^{-6}$ and 3×10^{-5} Ha, respectively. Under sampling noise, the spread across optimizers increases markedly. After high-shot reevaluation, gradient descent, SPSA, and CMAES yield the lowest corrected mean errors, all near 4 – 7×10^{-4} Ha, while BFGS, Nelder–Mead, and COBYLA degrade to the millihartree range (2 – 4×10^{-3} Ha). PSO remains competitive ($\sim 6 \times 10^{-4}$ Ha), showing resilience to noise despite its slower noiseless convergence. These results reveal that in H_2 , all optimizers succeed in the noiseless limit, but under realistic sampling conditions, stochastic and population-based methods retain sub-millihartree accuracy, whereas deterministic gradient-based ones lose stability.

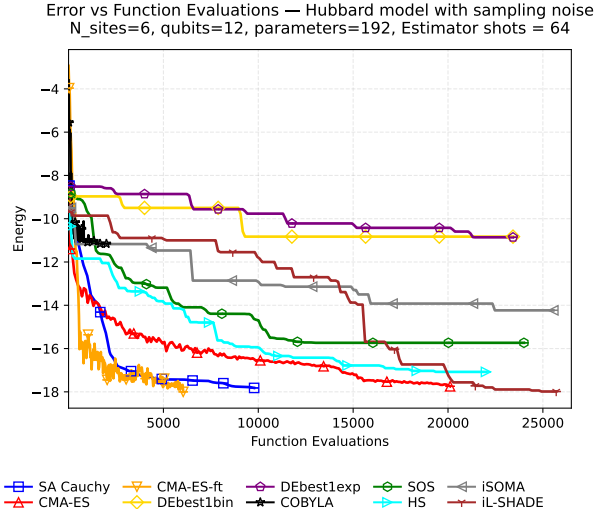


Fig. 4: Convergence comparison for the six-site Hubbard model using 64-shot estimation. Adaptive metaheuristics (iL-SHADE and CMAES) maintain stable progress where gradient-based and basic Differential Evolution variants stagnate.

The increase in system complexity for H_4 further separates optimizer performance. In statevector runs, BFGS, COBYLA, and SLSQP achieve errors of $\sim 7 \times 10^{-3}$ Ha, while CMAES and Nelder–Mead converge more slowly, and gradient descent reaches $\sim 2.5 \times 10^{-2}$ Ha. When sampling noise is introduced, the corrected high-shot results show that CMAES gives the lowest mean error (2.3×10^{-2} Ha), closely followed by PSO (2.7×10^{-2} Ha) and gradient descent (3.0×10^{-2} Ha). SPSA and COBYLA lie in the intermediate range ($3.5\text{--}3.8 \times 10^{-2}$ Ha), while BFGS and Nelder–Mead deteriorate strongly (above 4.5×10^{-2} Ha). Thus, for H_4 , gradient-based methods lose their noiseless advantage, and only population-based and stochastic algorithms retain partial accuracy.

For the full LiH molecule, the higher-dimensional ansatz amplifies these trends. In statevector simulations, BFGS, CMAES, COBYLA, Nelder–Mead, and SPSA reach errors near 4×10^{-3} Ha, while PSO and gradient descent are less precise (9×10^{-3} and 2×10^{-2} Ha). Under noise, CMAES achieves the best corrected mean error ($\sim 8 \times 10^{-3}$ Ha), followed by PSO (1.3×10^{-2} Ha) and SPSA (1.6×10^{-2} Ha). All deterministic optimizers (BFGS, COBYLA, Nelder–Mead) cluster near 2×10^{-2} Ha, consistent with reduced robustness to stochastic gradients. These results indicate that population-based and stochastic optimizers maintain sub-20 mHa accuracy even for larger systems, while deterministic gradient methods fail to scale effectively.

The LiH active space demonstrates the benefit of orbital truncation, both in optimizer cost and noise resilience. In the noiseless setting, all algorithms

achieve sub-millihartree accuracy, with CMAES, PSO, Nelder–Mead, and SPSA converging below 2×10^{-4} Ha, and BFGS and COBYLA reaching $\sim 2 \times 10^{-4}$ Ha. Under sampling noise, high-shot reevaluation reveals CMAES as the best performer (2.6×10^{-4} Ha), followed by SPSA (3.9×10^{-4} Ha), PSO (4.2×10^{-4} Ha), and Nelder–Mead (5.3×10^{-4} Ha). COBYLA and BFGS yield slightly higher errors (8×10^{-4} – 1.1×10^{-3} Ha), while gradient descent deteriorates to several millihartree and SLSQP diverges beyond 3×10^{-1} Ha. Active space reduction thus improves stability by roughly an order of magnitude relative to the full system.

Overall, the results across all four systems, summarized in Fig. 5, show a consistent evolution in optimizer behavior. In small, smooth landscapes (H_2), deterministic methods such as BFGS excel, but as system size and noise increase (H_4 , LiH), stochastic and population-based optimizers CMAES, PSO, and SPSA become dominant, achieving the lowest corrected errors and most stable convergence profiles. High-shot reevaluation proves indispensable, as apparent low-energy results from noisy runs often overestimate true accuracy. These findings emphasize a clear transition from curvature-driven optimization in noiseless low-dimensional systems to noise-resilient exploration strategies in larger, stochastic quantum simulations.

4 Conclusion

This work establishes a quantitative connection between measurement noise and optimizer instability in variational quantum algorithms. By benchmarking eight classical optimizers across molecular and condensed matter domains, we show that finite-shot sampling alone (without coherent or gate errors) is sufficient to destroy the deterministic structure of the variational landscape. The practical result is that gradient curvature becomes comparable to the noise amplitude, rendering gradient and Hessian information statistically meaningless.

Our main contribution is the systematic identification of where and why traditional optimizers fail. We demonstrate that deterministic gradient-based methods (BFGS, SLSQP) lose reliability once curvature signals fall below the sampling variance; they transition from contracting toward a minimum to simple random diffusion. Conversely, adaptive population based algorithms such as CMAES and iL-SHADE remain operational by implicitly averaging noise, which provides a general strategy for stochastic stability.

We also reveal a unique artifact to noisy quantum optimization: the winner’s curse, where statistical minima appear to fall below the true ground state energy. Our LiH study confirms that this bias can misleadingly suggest that noise is beneficial. This false advantage is removed by high-shot reevaluation, proving that the effect arises from estimator variance rather than physical noise assisted convergence. A statistically sound correction is to reevaluate elite individuals or track population means or trimmed means instead of relying on a single best sample.

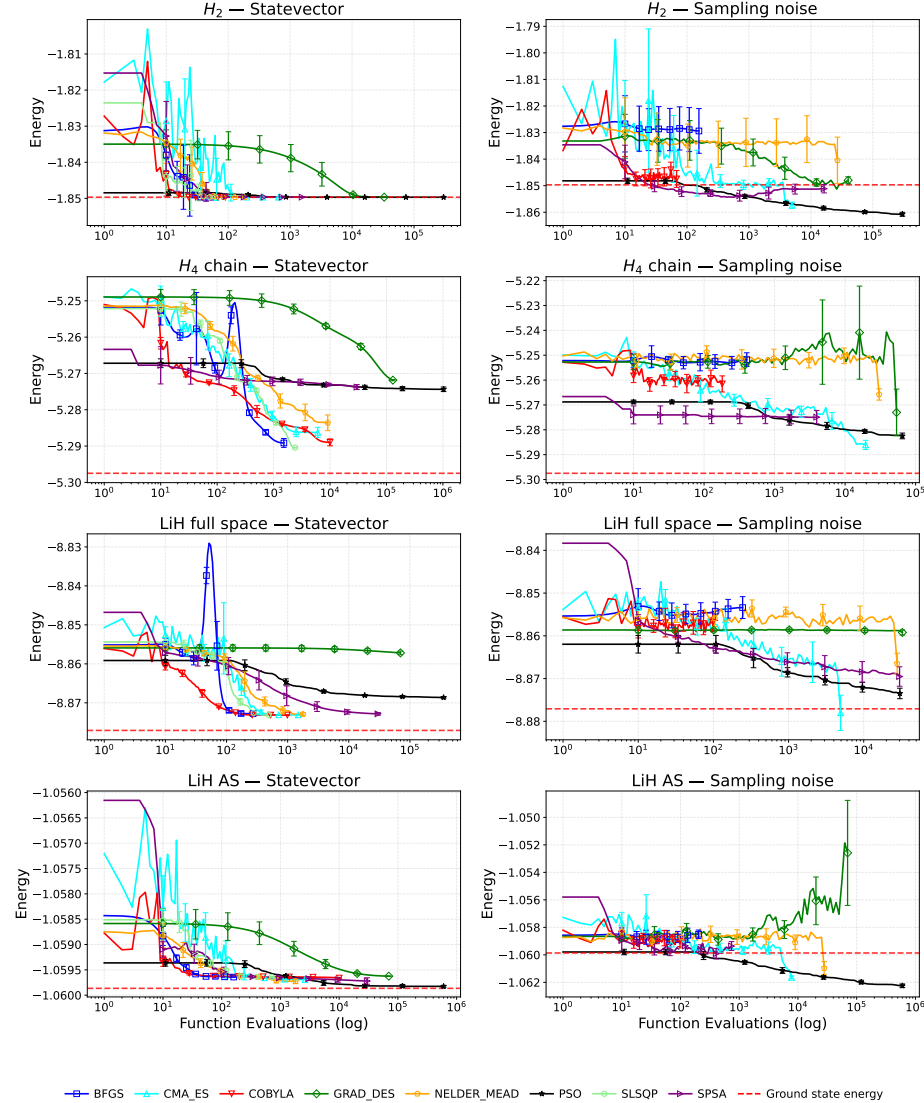


Fig. 5: Convergence curves for H_2 , H_4 , and LiH in full and active space with random initialization starts using tVHA. Finite-shot sampling increases variance and erases the performance gap between deterministic and evolutionary optimizers. In the right panel we can see optimizers convergence to dip below ground state energies (red dashed line).

From these analyzes, the reader can extract four practical takeaways for robust VQE optimization. First, structured ansatz as intrinsic noise mitigation. Compact, physically motivated designs such as tVHA maintain polynomially decaying gradients and stable curvature, reducing barren plateaus and noise sensitivity. Barren Plateaus are still a very active area of research, and further work will use a preferred, but more theoretically demanding, method for detecting BPs by analytically studying the scaling of the variance. For example, if $U(\theta)$ is a deep unitary circuit whose distribution of unitaries forms at least a 2-design over a Lie group, one can use representation theory to exactly evaluate the variances via Weingarten calculus.

Second, evolutionary optimizers are designed to overcome multimodal, rotated, shifted, and compositionally complex benchmark functions, similar to the rugged and noisy landscapes characteristic of VQE cost surfaces. As shown in IEEE CEC benchmarks [11], this robustness comes at the cost of increased function evaluations. However, this trade off can be advantageous in hybrid quantum-classical workflows. Methods such as iL-SHADE and CMAES converged to nearly exact values even for the multimodal Hubbard model under heavy noise (64 shots). This behavior suggests a resource efficient optimization strategy where low shot evaluations are used throughout most of the process, with adaptive shot increases only near convergence to refine high-precision results.

Third, adaptive metaheuristics tend to have the best results in all our experiments. Algorithms that self-adapt their search parameters, such as CMAES that updates its sampling distribution, and iL-SHADE that adaptively modifies its population size, crossover probability, and step size based on historical success, outperform static gradient-free, deterministic methods, and basic metaheuristics in the presence of noise.

Fourth, dimensionality reduction as noise control. Simplifying the variational space through active space truncation or feature pruning directly lowers the effective noise floor, often improving optimizer reliability by an order of magnitude.

This study focused exclusively on finite-shot sampling noise and does not include any form of quantum hardware noise. In future work, we will study how different types of noise, including hardware decoherence, thermal relaxation, and readout errors, contribute to the problems analyzed in this study.

Acknowledgments

Vojtěch Novák is supported by Grant of SGS No. SP2025/072, VSB-Technical University of Ostrava, Czech Republic. This work was supported by the Ministry of Education, Youth and Sports of the Czech Republic through the e-INFRA CZ (ID:90254). Martin Beseda is supported by Italian Government (Ministero dell'Università e della Ricerca, PRIN 2022 PNRR) – cod.P2022SEL7: "RECHARGE: monitoRing, tEsting, and CHaracterization of performAnce Regressions" – Decreto Direttoriale n. 1205 del 28/7/2023.

Data availability

To support tVHA findings and ensure reproducibility, we have published the dataset containing both the computed results and the scripts used to generate them. The dataset serves as a companion resource to this work and facilitates further research in hybrid quantum-classical architectures. It is publicly available on Zenodo [4].

Hubbard and Ising models simulations were conducted using a locally developed code, which is openly available for further examination and reproduction of results. The code, along with detailed Jupyter notebooks, can be accessed at ⁷.

Further details are available through the corresponding author.

A Experiment details

We performed large-scale simulations of the tVHA on classical hardware to assess optimization performance in quantum chemistry settings. Four molecular systems H_2 , LiH (full space), LiH (active space), and the H_4 chain were optimized using eight classical algorithms: BFGS [26], CMAES [14, 13], COBYLA [37], Gradient Descent, Nelder–Mead [29], PSO [10], SLSQP [5], and SPSA [38]. Each optimizer–molecule pair was evaluated in 20 independent runs (10 noiseless, 10 noisy) under random parameter initialization, yielding 640 total simulations with up to 10,000 iterations per run. Noisy configurations used 6144 measurement shots per function evaluation.

Initial parameters were drawn independently from a uniform $[0, 1]$ distribution using `numpy.random.rand`, and pseudorandom seeds were not fixed to preserve stochastic independence across runs. Each optimizer employed its standard termination criterion and default hyperparameters to ensure comparability. All implementations used a controlled Python environment combining `qiskit` 1.0.2 [22], `qiskit_nature` 0.7.2, `qiskit_aer` 0.14.2, `pyscf` 2.6.0 [39], `scipy` 1.15.2 [43], and `cma` 3.3.0 [14], with full source and logs available on Zenodo [4].

For the Ising and Hubbard models, we have used optimizers: CMAES, COBYLA, DEbest1bin and DEbest1exp both from `scipy` [43], SA Cauchy, iL-SHADE from `PyADE` [48], HS [49] and SOS [8] from `mealpy` [41, 42], iSOMA [50]. For each setting, we performed five independent runs and report the mean results for both function evaluations (FEs) and convergence.

The CMAES optimizer was further fine-tuned using the IRACE method. In contrast, iL-SHADE did not require additional tuning due to its self-adjusting nature, utilizing success-history-based parameter adaptation and a linear population size reduction scheme. For further details on hyperparameters, refer to [32] or ⁸.

⁷ <https://github.com/VojtechNovak/VQAEvolutionary>

⁸ <https://github.com/VojtechNovak/VQAEvolutionary>

References

1. Andrews, I., Kasy, M.: Identification of and inference on winners: Statistical inference after model selection. *Econometrica* **87**(2), 465–506 (2019). <https://doi.org/10.3982/ECTA15310>
2. Andrews, I., Kasy, M.: Identification of and correction for publication bias. *American Economic Review* **109**(8), 2766–2794 (2021). <https://doi.org/10.1257/aer.20180310>
3. Beseda, M., Illésová, S., Yalouz, S., Senjean, B.: State-averaged orbital-optimized vqe: A quantum algorithm for the democratic description of ground and excited electronic states. *arXiv preprint arXiv:2401.11884* (2024)
4. Beseda, M., Illésová, S., Possel, C., Bezděk, T., Novák, V.: Numerical optimization strategies for the variational hamiltonian ansatz in noisy quantum environments: Results (2025), <https://doi.org/10.5281/zenodo.15526170>
5. Boggs, P.T., Tolle, J.W.: Sequential quadratic programming. *Acta numerica* **4**, 1–51 (1995), <https://doi.org/10.1017/S0962492900002518>
6. Bonet-Monroig, X., Wang, H., Vermetten, D., Senjean, B., Moussa, C., Bäck, T., Dunjko, V., O'Brien, T.E.: Performance comparison of optimization methods on variational quantum algorithms. *arXiv preprint arXiv:2111.13454* (2021)
7. Cerezo, M., Arrasmith, A., Babbush, R., Benjamin, S.C., Endo, S., Fujii, K., McClean, J.R., Mitarai, K., Yuan, X., Cincio, L., et al.: Variational quantum algorithms. *Nature Reviews Physics* **3**(9), 625–644 (2021)
8. Cheng, M.Y., Prayogo, D.: Symbiotic organisms search: A new metaheuristic optimization algorithm. *Computers & Structures* **139**, 98–112 (2014), <https://www.sciencedirect.com/science/article/pii/S0045794914000881>
9. Ciaramelletti, C., Beseda, M., Consiglio, M., Lepori, L., Apollaro, T.J.G., Paganelli, S.: Detecting quasidegenerate ground states in topological models via the variational quantum eigensolver. *Phys. Rev. A* **111**, 022437 (Feb 2025), <https://link.aps.org/doi/10.1103/PhysRevA.111.022437>
10. Eberhart, R., Kennedy, J.: Particle swarm optimization. In: Proceedings of the IEEE international conference on neural networks. vol. 4, pp. 1942–1948. Citeseer (1995), <https://doi.org/10.1109/ICNN.1995.488968>
11. García-Martínez, C., Gutiérrez, P.D., Molina, D., Lozano, M., Herrera, F.: Since cec 2005 competition on real-parameter optimisation: a decade of research, progress and comparative analysis's weakness. *Soft Computing* **21**(19), 5573–5583 (2017)
12. Gupta, M.K., Beseda, M., Gawron, P.: How quantum computing-friendly multispectral data can be? In: IGARSS 2022 - 2022 IEEE International Geoscience and Remote Sensing Symposium. pp. 4153–4156 (2022). <https://doi.org/10.1109/IGARSS46834.2022.9883676>
13. Hansen, N.: The cma evolution strategy: a comparing review. Towards a new evolutionary computation: Advances in the estimation of distribution algorithms pp. 75–102 (2006)
14. Hansen, N., Akimoto, Y., Baudis, P.: Cma-es/pycma on github (February 2019). <https://doi.org/10.5281/zenodo.2559634>, <https://doi.org/10.5281/zenodo.2559634>
15. Horáčková, L., Kojecký, L., Fiore, U., Vozňák, M., Zelinka, I.: Evolving quantum circuits: isoma-driven synthesis of toffoli gates. In: Proceedings of the 27th International Conference on Modeling, Analysis and Simulation of Wireless and Mobile Systems. MSWiM '25, Association for Computing Machinery (2025)

16. Hubbard, J.: Electron correlations in narrow energy bands. *Proceedings of the Royal Society of London. Series A. Mathematical and Physical Sciences* **276**(1365), 238–257 (1963). <https://doi.org/10.1098/rspa.1963.0204>, <http://doi.org/10.1098/rspa.1963.0204>
17. Illésová, S., Rybotycki, T., Beseda, M.: Qmetric: Benchmarking quantum neural networks across circuits, features, and training dimensions. *arXiv preprint arXiv:2506.23765* (2025)
18. Illésová, S., Rybotycki, T., Gawron, P., Beseda, M.: On the importance of fundamental properties in quantum-classical machine learning models. *arXiv preprint arXiv:2507.10161* (2025)
19. Illésová, S., Beseda, M., Yalouz, S., Lasorne, B., Senjean, B.: Transformation-free generation of a quasi-diabatic representation from the state-average orbital-optimized variational quantum eigensolver. *Journal of Chemical Theory and Computation* **21**(11), 5457–5480 (2025). <https://doi.org/10.1021/acs.jctc.5c00327>
20. Illésová, S., Novák, V., Bezděk, T., Possel, C., Beseda, M.: Numerical optimization strategies for the variational hamiltonian ansatz in noisy quantum environments (2025), <https://arxiv.org/abs/2505.22398>
21. Illésová, S., Bezděk, T., Novák, V., Senjean, B., Beseda, M.: Statistical benchmarking of optimization methods for variational quantum eigensolver under quantum noise (2025), <https://arxiv.org/abs/2510.08727>
22. Javadi-Abhari, A., Treinish, M., Krsulich, K., Wood, C.J., Lishman, J., Gacon, J., Martiel, S., Nation, P.D., Bishop, L.S., Cross, A.W., Johnson, B.R., Gambetta, J.M.: Quantum computing with qiskit (2024). <https://doi.org/10.5281/zenodo.2562111>
23. Kraft, D.: A software package for sequential quadratic programming. *Forschungsbericht- Deutsche Forschungs- und Versuchsanstalt fur Luft- und Raumfahrt* (1988)
24. Larocca, M., Thanasilp, S., Wang, S., Sharma, K., Biamonte, J., Coles, P.J., Cinicio, L., McClean, J.R., Holmes, Z., Cerezo, M.: A review of barren plateaus in variational quantum computing (2025), *arXiv preprint arXiv:2405.00781*
25. Lieb, E., Schultz, T., Mattis, D.: Two soluble models of an antiferromagnetic chain. *Annals of Physics* **16**(3), 407–466 (1961)
26. Liu, D.C., Nocedal, J.: On the limited memory bfgs method for large scale optimization. *Mathematical Programming* **45**, 503–528 (1989)
27. Marini, F., Walczak, B.: Particle swarm optimization (pso). a tutorial. *Chemometrics and intelligent laboratory systems* **149**, 153–165 (2015)
28. McClean, J.R., Boixo, S., Smelyanskiy, V.N., Babbush, R., Neven, H.: The theory of variational hybrid quantum–classical algorithms. *npj Quantum Information* **5**, 75 (2019). <https://doi.org/10.1038/s41534-019-0197-3>
29. Nelder, J.A., Mead, R.: A simplex method for function minimization. *The computer journal* **7**(4), 308–313 (1965). <https://doi.org/10.1093/comjnl/7.4.308>
30. Novák, V., Zelinka, I., Přibylová, L., Martínek, L., Benčurik, V.: Predicting post-surgical complications with quantum neural networks: A clinical study on anastomotic leak. *arXiv preprint arXiv:2506.01708* (2025)
31. Novák, V., Zelinka, I., Přibylová, L., Martínek, L.: Quantum neural networks for propensity score estimation and survival analysis in observational biomedical studies (2025), <https://arxiv.org/abs/2506.19973>
32. Novák, V., Zelinka, I., Snášel, V.: Optimization strategies for variational quantum algorithms in noisy landscapes (2025), <https://arxiv.org/abs/2506.01715>
33. Park, C.Y., Killoran, N.: Hamiltonian variational ansatz without barren plateaus. *Quantum* **8**, 1239 (Feb 2024), <https://doi.org/10.22331/q-2024-02-01-1239>

34. Possel, C., Hahn, W., Shirazi, R., Walt, M., Pinski, P., Wilhelm, F.K., Bagrets, D.: Truncated variational hamiltonian ansatz: efficient quantum circuit design for quantum chemistry and material science. arXiv preprint arXiv:2505.19772 (2025)
35. Rajamani, A., Beseda, M., Lasorne, B., Senjean, B.: How an equi-ensemble description systematically outperforms the weighted-ensemble variational quantum eigensolver (2025), <https://arxiv.org/abs/2509.17982>
36. Rakshit, S., Das, S., Suganthan, P.N.: Noisy evolutionary optimization algorithms: A comprehensive survey. *Swarm and Evolutionary Computation* **33**, 18–45 (2017). <https://doi.org/10.1016/j.swevo.2016.10.003>
37. Regis, R.G.: Stochastic radial basis function algorithms for large-scale optimization involving expensive black-box objective and constraint functions. *Computers & Operations Research* **38**(5), 837–853 (2011)
38. Spall, J.C.: Implementation of the simultaneous perturbation algorithm for stochastic optimization. *IEEE Transactions on Aerospace and Electronic Systems* **34**(3), 817–823 (1998). <https://doi.org/10.1109/7.705889>
39. Sun, Q., Berkelbach, T.C., Blunt, N.S., Booth, G.H., et al.: Pyscf: the python-based simulations of chemistry framework. *Wiley Interdisciplinary Reviews: Computational Molecular Science* **8**(1), e1340 (2018), <https://doi.org/10.1002/wcms.1340>
40. Trovato, A., Beseda, M., Di Nucci, D.: A preliminary investigation on the usage of quantum approximate optimization algorithms for test case selection. arXiv preprint arXiv:2504.18955 (2025)
41. Van Thieu, N., Barma, S.D., Van Lam, T., Kisi, O., Mahesha, A.: Groundwater level modeling using augmented artificial ecosystem optimization. *Journal of Hydrology* **617**, 129034 (2023). <https://doi.org/10.1016/j.jhydrol.2022.129034>
42. Van Thieu, N., Mirjalili, S.: Mealpy: An open-source library for latest meta-heuristic algorithms in python. *Journal of Systems Architecture* (2023). <https://doi.org/10.1016/j.sysarc.2023.102871>
43. Virtanen, P., Gommers, R., Oliphant, T.E., et al.: SciPy 1.0: Fundamental Algorithms for Scientific Computing in Python. *Nature Methods* **17**, 261–272 (2020). <https://doi.org/10.1038/s41592-019-0686-2>
44. Vorwerk, C., Sheng, N., Govoni, M., Huang, B., Galli, G.: Quantum embedding theories to simulate condensed systems on quantum computers. *Nature Computational Science* **2**(7), 424–432 (2022)
45. Wang, S., Fontana, E., Cerezo, M., Sharma, K., Sone, A., Cincio, L., Coles, P.J.: Noise-induced barren plateaus in variational quantum algorithms. *Nature Communications* **12**(6961) (2020). <https://doi.org/10.1038/s41467-020-21700-3>
46. Wierichs, D., Gogolin, C., Kastoryano, M.: Avoiding local minima in variational quantum eigensolvers with the natural gradient optimizer. *Phys. Rev. Res.* **2**, 043246 (Nov 2020), <https://link.aps.org/doi/10.1103/PhysRevResearch.2.043246>
47. Wiersema, R., Zhou, C., de Sereville, Y., Carrasquilla, J.F., Kim, Y.B., Yuen, H.: Exploring entanglement and optimization within the hamiltonian variational ansatz. *PRX Quantum* **1**, 020319 (Dec 2020), <https://link.aps.org/doi/10.1103/PRXQuantum.1.020319>
48. xKuZz: Pyade: Python advanced differential evolution. GitHub repository (2025), <https://github.com/xKuZz/pyade>
49. Yang, X.S.: Harmony search as a metaheuristic algorithm. In: *Music-inspired harmony search algorithm: theory and applications*, pp. 1–14. Springer (2009)
50. Zelinka, I., Kojecký, L., Lampart, M., Nowaková, J., Plucar, J.: isoma swarm intelligence algorithm in synthesis of quantum computing circuits. *Applied Soft Computing* **142**, 110350 (2023), <https://www.sciencedirect.com/science/article/pii/S156849462300368X>